Introduction

Oxidative stress is implicated in the pathogenesis of hypertension (1,2). Among the target organs of hypertensive vascular diseases, the brain is the most affected by oxidative stress (3,4). Previously, we demonstrated that the generation of reactive oxygen species (ROS) is enhanced in the rostral ventrolateral medulla (RVLM) of the brain stem (i.e., where the vasomotor center is located) of stroke-prone spontaneously hypertensive rats (SHRSP), and that the oxidative stress in the RVLM induces a sympatho-excitatory effect (5). These findings suggest that oxidative stress in the RVLM is an important target in the treatment of hypertension.

The 3-hydroxy-3-methylglutaryl coenzyme A (HMG-CoA) reductase inhibitors (statins) are potent inhibitors of cholesterol biosynthesis. These agents slow the progression and foster the regression of atherosclerosis, resulting in an improvement of cardiovascular outcomes in humans with elevated and normal serum cholesterol levels (6–9). Moreover, statins might activate endothelial nitric oxide synthase (eNOS), improve endothelial function, increase vascular nitric oxide (NO) bioavailability, reduce oxidative stress, and improve endothelial progenitor cell function as a pleiotropic effect (10–19). In humans, four weeks of simvastatin treatment improves endothelial function independently of the decreases in LDL cholesterol, at least in part by reducing oxidative stress (20). The oral administration of atorvastatin has sympatho-inhibitory effects in SHRSP via an increase in NO production with upregulation of eNOS in the brain (21). The increase in NO production in the brain is thought to be mediated not only by eNOS upregulation in the brain by atorvastatin, but also by the antioxidant effect of atorvastatin, because NO is scavenged by ROS and statin has an antioxidant effect (10–19). Therefore, the aim of the present study was to determine if atorvastatin reduces oxidative stress in the RVLM of SHRSP along with the sympatho-inhibitory effect.

Materials and Methods

This study was reviewed and approved by the committee on ethics of Animal Experiments, Kyushu University Graduate School of Medical Sciences, and conducted according to the Guidelines for Animal Experiments of Kyushu University.

Measurements of Blood Pressure, Heart Rate, and Urinary Norepinephrine Excretion

Male Wister-Kyoto (WKY)/Izm and SHRSP/Izm (15 weeks old, SLC Japan, Hamamatsu, Japan) were put on standard feed or on standard feed supplemented with atorvastatin (gift from Pfizer Pharmaceuticals Inc.) and had free access to drinking water. The animals received atorvastatin at a dose of 50 mg/kg body weight per day, which was calculated according to the daily food intake (11,21), for 30 days. In rats, this dose produces plasma concentrations that are comparable to those achieved after the oral administration of similar doses of atorvastatin in humans (22). Systolic blood pressure (SBP) and heart rate (HR) were recorded using the tail-cuff method. Urine was collected for 24 hours using a metabolic cage, as described in our previous studies (5,21,23–26). Urinary norepinephrine was measured for 24 hours as a parameter of sympathetic nerve activity (5,21,23–26). To obtain RVLM tissues, the rats were deeply anesthetized with sodium pentobarbital (100 mg/kg IP) and transcardially perfused with phosphate buffered saline (5,21). The brain was removed quickly, and

1 mm-thick sections were obtained with a cryostat (5). The RVLM was defined according to a rat brain atlas (27), and the RVLM tissue was obtained using the micro-punch technique (5).

Measurement of TBARS Levels in the RVLM and Whole Brain

Thiobarbituric acid-reactive substances (TBARS) level was measured as a parameter of oxidative stress in the RVLM and whole brain (3,5). The RVLM and whole brain tissues were homogenized in 1.15% KCl (pH 7.4), 0.4% sodium dodecyl sulfate, and 7.5% acetic acid adjusted to pH 3.5 with NaOH. Thiobarbituric acid (0.3%) was added to the homogenate. The mixture was maintained at 5°C for 60 minutes, followed by heating to 100°C for 60 minutes. After cooling, the mixture was extracted with distilled water and *n*-butanolpyridine (15:1) and centrifuged at 1600*g* for 10 minutes. The absorbance of the organic phase was measured at 532 nm. The amount of TBARS was determined by absorbance with a molecular extinction coefficient of 156 000 and expressed as μmol/g wet wt. All values were expressed as the mean ± SEM, and unpaired Student's *t*-test was performed to compare the atorvastatin-treated and the control groups. p values of less than 0.05 were considered significant.

Results

Effects of Atorvastatin on Blood Pressure, Heart Rate, and Urinary Norepinephrine Excretion

Prior to treatment with atorvastatin, SBP, HR, and urinary norepinephrine excretion were significantly higher in SHRSP than in WKY (194 ± 4 mmHg vs. 139 ± 6 mmHg, 388 ± 11 beats/min vs. 348 ± 22 beats/min, 1.38 ± 0.06 μg vs. 0.91 ± 0.06 μg, $p < .05$; n = 5 for each). After 30 days, SBP and urinary norepinephrine excretion in SHRSP were significantly lower in the atorvastatin-treated group than in the control group (173 ± 9 mmHg vs. 199 ± 6 mmHg, 1.07 ± 0.07 μg vs. 1.41 ± 0.04 μg; $p < .05$, n = 5 for each; see Figure 1). After 30 days in WKY, however, there was no significant difference in SBP and urinary norepinephrine excretion between the atorvastatin-treated group and the control group. HR was not significantly different between the atorvastatin-treated group and the control group in SHRSP and WKY (SHRSP: 384 ± 13 beats/min vs. 372 ± 18 beats/min; WKY: 352 ± 26 beats/min vs. 336 ± 24 beats/min).

Effects of Atorvastatin on TBARS Levels in RVLM and Whole Brain

Prior to treatment with atorvastatin, TBARS levels were significantly higher in the RVLM and whole brain of SHRSP than WKY (RVLM: 0.78 ± 0.06 vs. 0.32 ± 0.06 μmol/g wet wt; whole brain: 0.88 ± 0.06 vs. 0.42 ± 0.08 μmol/g wet wt, $p < .05$; n = 5 for each). After 30 days, TBARS levels of RVLM and whole brain in SHRSP were significantly lower in the atorvastatin-treated group than in the control group (RVLM: 0.55 ± 0.03 μmol/g wet wt vs. 0.75 ± 0.04 μmol/g wet wt; whole brain: 0.63 ± 0.04 μmol/g wet wt vs 0.84 ± 0.07 μmol/g wet wt; $p < .05$, n = 5 for each; see Figure 2). After 30 days in WKY, however, there was no significant difference in TBARS levels of RVLM and whole brain between the atorvastatin-treated group and the control group.

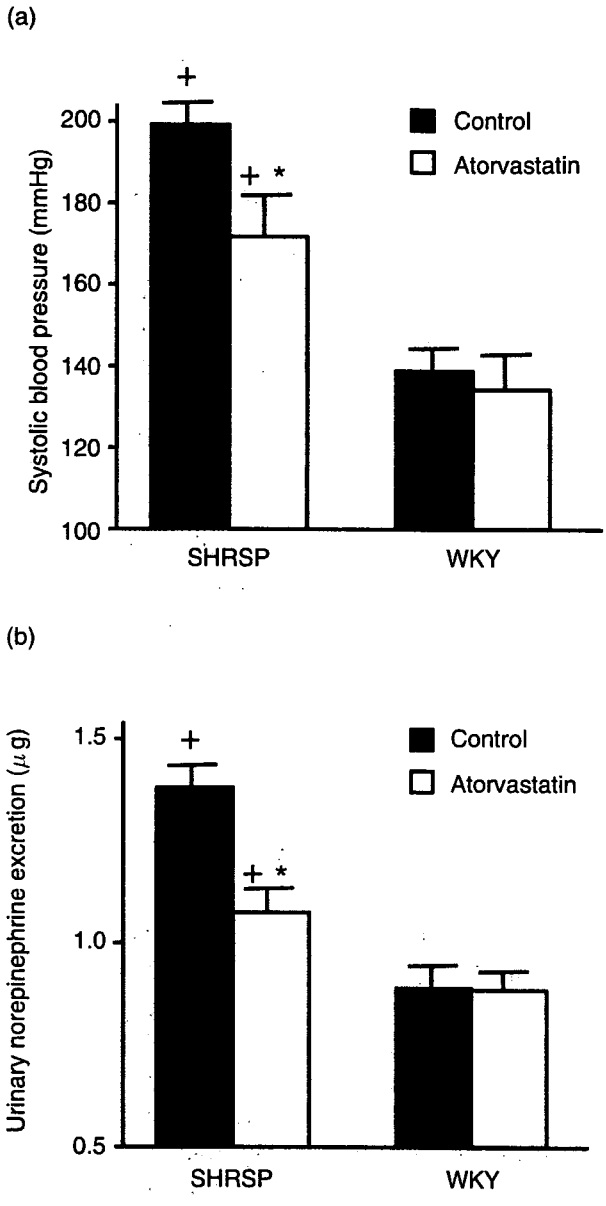

Figure 1. Effects of treatment with atorvastatin for 30 days on (A) systolic blood pressure, and (B) 24-hour urinary norepinephrine excretion in SHRSP and WKY. Male SHRSP and WKY (15 weeks old) were placed on a standard feed diet (control, filled square) or on a standard feed diet supplemented with atorvastatin (50 mg/kg of body weight per day, open square) for 30 days. Systolic blood pressure was assessed with rats in the conscious state using the tail-cuff method. Urinary norepinephrine excretion over 24 hours was measured by high performance liquid chromatography. Data are shown as mean ± SEM (n = 5 per group). *$p < .05$ versus control group in the same strain; $^{\dagger}p < .05$ versus control group in WKY rats after 30 days.

Discussion

The major finding of the present study was that atorvastatin reduced oxidative stress, as measured by a reduction in TBARS levels, in the RVLM of SHRSP, which was significantly increased in SHRSP compared with WKY, and that the antioxidant effect of atorvastatin contributes to the sympatho-inhibitory effect of atorvastatin.

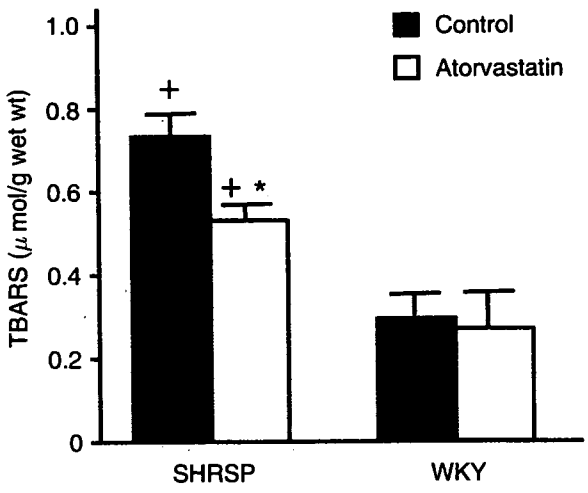

Figure 2. Effects of treatment with atorvastatin for 30 days on TBARS levels in the RVLM of SHRSP and WKY. Male SHRSP and WKY (15 weeks old) were placed on a standard feed diet (control, filled square) or on a standard feed diet supplemented with atorvastatin (50 mg/kg of body weight per day, open square) for 30 days. Data are shown as mean ± SEM (n = 5 per group). $^{*}p < .05$ versus control group in the same strain, $^{\dagger}p < .05$ versus control group in WKY rats after 30 days.

We previously demonstrated that the oral administration of atorvastatin decreased blood pressure in SHRSP (21), and the results of the present study are consistent with those of the previous study. We also suggested that the decrease in blood pressure was due to the sympatho-inhibitory effects of atorvastatin via an increase in NO production in the brain (21). Furthermore, a recent study suggests that oxidative stress in the RVLM increases sympathetic nerve activity (5). Statins have antioxidant effects (10–19,28–29), and alterations in the balance between NO and superoxide are implicated in hypertension (30–31). Statins increase thioredoxin activity by an NO-dependent pathway (32), which might be another mechanism through which improved NO availability promotes endogenous vascular antioxidant defense systems. Statin treatment inhibits the activation of the oxidant enzyme system NAD (P) H oxidase, likely by preventing a membrane translocation of the small G protein rac-1 (15,33), which might contribute to reduced vascular oxidant stress after statin treatment. These studies suggest that statin upregulates NO bioavailability and has antioxidant effects. The RVLM is known as the vasomotor center, and NO and oxidative stress in the RVLM are important factors regulating the sympathetic nerve activity (5,23–26). These results suggest that the oral administration of atorvastatin has antioxidant effects in the RVLM of SHRSP as a pleiotropic effect, and these antioxidant effects induce the upregulation of NO production in the RVLM of SHRSP, as well as sympatho-inhibitory effects. Furthermore, statins enhance endothelial NO bioavailability by both promoting endothelial NO production (14,34–36) and preventing NO inactivation by radicals (15). The decreases in oxidative stress by the oral administration of atorvastatin in the RVLM are thought to induce a sympatho-inhibitory effect because oxidative stress in the RVLM causes sympatho-excitatory effects (5).

Recent clinical and animal studies suggest that statins exert protective effects against nonhemorrhagic stroke (37–39). Moreover, statins improve the outcome of acute ischemic stroke in humans (37). In SHRSP, rosuvastatin attenuates inflammatory processes associated with cerebrovascular disease by increasing the transcription of

eNOS mRNA, preventing endothelial dysfunction, reducing production of ROS, and inhibiting leukocyte-endothelial adhesion (40). Furthermore, statins improve the outcome after myocardial infarction or stroke by LDL cholesterol-independent, eNOS-dependent mechanisms (10,41,42). In this study, the antioxidant effects of atorvastatin were not specific in the RVLM and we confirmed that atorvastatin has antioxidant effects in the whole brain. We demonstrated that sympathetic nerve activity was increased in the SHRSP (5,21) and a previous study reported that the densities of noradrenergic nerve fibers in the epicardium and myocardium are significantly higher in SHRSP than in WKY (37). The sympatho-inhibitory effects of atorvastatin might also contribute to the protective effects against stroke.

We measured TBARS levels as the parameter of oxidative stress in the brain. TBARS levels are widely used as a marker of oxidative stress (3–5). TBARS levels, however, are an indirect marker of oxidative stress. Previously, we directly measured oxidative stress in the brain of SHRSP and WKY using electron spin resonance spectroscopy and confirmed that TBARS levels are comparable to the levels of oxidative stress measured by electron spin resonance spectroscopy in the brain (5). These results suggest that TBARS levels are a valid parameter of oxidative stress in the brain.

In the present study, we used atorvastatin only and did not perform experiments to examine the effect of other statins. It is not known whether the antioxidant effect of atorvastatin in the brain is a specific effect of atorvastatin or a general effect of all statins. Further studies are necessary.

Conclusion

The oral administration of atorvastatin for 30 days reduced blood pressure, urinary norepinephrine excretion, and TBARS levels in the RVLM of SHRSP. These results suggest that the antioxidant effect of atorvastatin in the RVLM might contribute to the sympatho-inhibitory effects in SHRSP through the upregulation of NO bioavailability by the scavenger effect of oxidative stress against NO and the decrease in the sympatho-excitatory effect of oxidative stress.

Acknowledgments

This work was supported by Grants-in-Aid for Scientific Research from the Japan Society for the Promotion of Science (C15590757, C17590745) and, in part, by the Health and Labor Sciences Research Grant for Comprehensive Research in Aging and Health Labor and Welfare of Japan.

References

1. Kerr S, Brosnan J, McIntyre M, Reid JL, Dominiczak AF, Hamilton CA. Superoxide anion production is increased in a model of genetic hypertension. *Hypertension.* 1999;33:1353–1358.
2. Nakazono K, Watanabe N, Matsuno K, Sakai J, Sato T, Inoue M. Does superoxide underlie the pathogenesis of hypertension? *Proc Natl Acad Sci USA.* 1991;88:10045–10048.
3. Ohtsuki T, Matsumoto M, Suzuki K, Taniguchi N, Kamada T. Mitochondrial lipid peroxidation and superoxide dismutase in rat hypertensive target organs. *Am J Physiol.* 1995;268:H1418–H1421.
4. Kimoto-Kinoshita S, Nishida S, Tomura TT. Age-related change of antioxidant capacities in the cerebral cortex and hippocampus of stroke-prone spontaneously hypertensive rats. *Neurosci Lett.* 1999;273:41–44.

5. Kishi T, Hirooka Y, Kimura Y, Ito K, Shimokawa H, Takeshita A. Increased reactive oxygen species in rostral ventrolateral medulla contribute to neural mechanisms of hypertension in stroke-prone spontaneously hypertensive rats. *Circulation.* 2004;109:2357–2362.
6. Randomized trial of cholesterol lowering in 4444 patients with coronary heart disease: The Scandinavian Simvastatin Survival study (4S). *Lancet.* 1994;344:1383–1389.
7. Prevention of cardiovascular events and death with pravastatin in patients with coronary heart disease and a broad range of initial cholesterol levels. The Long-Term Intervention with Pravastatin in Ischemic Disease (LIPID) Study Group. *N Engl J Med.* 1998;339:1349–1357.
8. Sever PS, Dahlof B, Poulter NR, Wedel H, Beevers G, Caulfield M, Nieminen M, O'Brien E, Ostergren J. Prevention of coronary and stroke events with atorvastatin in hypertensive patients who have average or lower-than-average cholesterol concentrations, in the Anglo-Scandinavian Cardiac Outcomes Trial-Lipid Lowering Arm (ASCOT-LLA): A multicentre randomized controlled trials. *Lancet.* 2003;361:1149–1158.
9. Glorioso N, Troffa C, Filigheddu F, Dettori F, Soro A, Parpaglia PP, Collatina S, Pahor M. Effect of the HMG-CoA reductase inhibitors on blood pressure in patients with essential hypertension and primary hypercholesterolemia. *Hypertension.* 1999;34:1281–1286.
10. Endres M, Laufs U, Huang Z, Nakamura T, Huang P, Moskowitz MA, Liao JK. Stroke protection by 3-hydroxy-3-methylglutaryl (HMG)-CoA reductase inhibitors mediated by endothelial nitric oxide synthase. *Proc Natl Acad Sci USA.* 1998;95:8880–8885.
11. Wassmann S, Laufs U, Baumer AT, Muller K, Ahlbory K, Linz W, Itter G, Rosen R, Bohm M, Nickenig G. HMG-CoA reductase inhibitors improve endothelial dysfunction in normocholesterolemic hypertension via reduced production of reactive oxygen species. *Hypertension.* 2001;37:1450–1457.
12. O'Driscoll G, Green D, Taylor RR. Simvastatin, an HMG-coenzyme A reductase inhibitor, improves endothelial function within one month. *Circulation.* 1997;95:1126–1131.
13. Mital S, Zhang X, Zhao G, Bernstein RD, Smith CJ, Fulton DL, Sessa WC, Liao JK, Hintze TH. Simvastatin upregulates coronary endothelial nitric oxide production conscious dogs. *Am J Physiol.* 2000;279:H2649–H2657.
14. Laufs U, LaFata V, Plutzky J, Liao JK. Upregulation of endothelial nitric oxide synthase by HMG-CoA reductase inhibitors. *Circulation.* 1998;97:1129–1135.
15. Wassmann S, Laufs U, Muller K, Konkol C, Ahlbory K, Baumer AT, Linz W, Bohm M, Nickenig G. Cellular antioxidant effects of atorvastatin in vitro and in vivo. *Arterioscler Thromb Vasc Biol.* 2002;22:300–305.
16. Laufs U, Liao JK. Isoprenoid metabolism and the pleiotropic effects of statins. *Curr Atheroscler Rep.* 2003;5:372–378.
17. Palinski W. New evidence for beneficial effects of statins unrelated to lipid lowering. *Atheroscler Thromb Vasc Biol.* 2001;21:3–5.
18. Llevadot J, Murasawa S, Kureishi Y, Uchida S, Masuda H, Kawamoto A, Walsh K, Isner JM, Asahara T. HMG-CoA reductase inhibitor mobilizes bone marrow-derived endothelial progenitor cells. *J Clin Invest.* 2001;108:399–405.
19. Vasa M, Fichtlscherer S, Adler K, Aicher A, Martin H, Zeiher AM, Dimmeler S. Increase in circulating endothelial progenitor cells by statin therapy in patients with stable coronary artery disease. *Circulation.* 2001;103:2885–2890.
20. Landmesser U, Bahlmann F, Mueller BS, Spiekermann S, Kirchhoff N, Schulz S, Manes C, Fischer D, De Groot K, Fliser D, Fauler G, Marz W, Drexler H. Simvastatin versus ezetimibe: Pleiotropic and lipid-lowering effects on endothelial function in humans. *Circulation.* 2005;111:2356–2363.
21. Kishi T, Hirooka Y, Mukai Y, Shimokawa H, Takeshita A. Atorvastatin causes depressor and sympatho-inhibitory effects with upregulation of nitric oxide synthases in stroke-prone spontaneously hypertensive rats. *J Hypertens.* 2003;21:379–386.
22. Hamilton CA, Brosnan MJ, McIntyre M, Graham D, Dominiczak AF. Superoxide excess in hypertension and aging. *Hypertension.* 2001;37:529–534.

23. Sakai K, Hirooka Y, Matsuo I, Eshima K, Shigematsu H, Shimokawa H, Takeshita A. Overexpression of eNOS in NTS causes hypotension and bradycardia in vivo. *Hypertension.* 2000;36:1023–1028.
24. Hirooka Y, Sakai K, Kishi T, Takeshita A. Adenovirus-mediated gene transfer into the NTS in conscious rats: a new approach to examining the central control of cardiovascular regulation. *Ann NY Acad Sci.* 2001;940:197–205.
25. Kishi T, Hirooka Y, Sakai K, Shigematsu H, Shimokawa H, Takeshita A. Overexpression of eNOS in the RVLM causes hypotension and bradycardia via GABA release. *Hypertension.* 2001;38:896–901.
26. Kishi T, Hirooka Y, Ito K, Sakai K, Shimokawa H, Takeshita A. Cardiovascular effects of overexpression of endothelial nitric oxide synthase in the rostral ventrolateral medulla in stroke-prone spontaneously hypertensive rats. *Hypertension.* 2002;39:264–268.
27. Paxinos G, Watson C. *The Rat Brain in Stereotaxic Coordinates.* New York: Academic Press; 1998.
28. Rikitake Y, Kawashima S, Takeshita S, Yamashita T, Azumi H, Yasuhara M, Nishi H, Inoue N, Yokoyama M. Anti-oxidative properties of fluvastatin, an HMG-CoA reductase inhibitor, contribute to prevention of atherosclerosis in cholesterol-fed rabbits. *Atherosclerosis.* 2001;154:87–96.
29. Thakur NK, Hayashi T, Sumi D, Kano H, Tsunekawa T, Iguchi A. HMG-CoA reductase inhibitor stabilizes rabbit atheroma by increasing basal NO and decreasing superoxide. *Am J Physiol.* 2001;281:H75–H83.
30. Delanty N, Vaughan CJ. Vascular effects of statins in stroke. *Stroke.* 1997;28:2315–2320.
31. The Long-Term Intervention with Pravastatin in Ischemic Disease (LIPID) Study Group. Prevention of cardiovascular events and death with pravastatin in patients with coronary heart disease and a broad range or initial cholesterol levels. *N Engl J Med.* 1998;339:1349–1357.
32. Haendeler J, Hoffmann J, Zeiher AM, Dimmler S. Antioxidant effects of statins via S-nitrosylation and activation of thioredoxin in endothelial cells: A novel vasculoprotective function of statins. *Circulation.* 2004;110:856–861.
33. Maack C, Kartes T, Kilter H, Schafers HJ, Nickenig G, Bohm M, Laufs U. Oxygen free radical release in human failing myocardium is associated with increased activity of rac1-GTPase and represents a target for statin treatment. *Circulation.* 2003;108:1567–1574.
34. Kureishi Y, Luo Z, Shiojima I, Bialik A, Fulton D, Lefer DJ, Sessa WC, Walsh K. The HMG-CoA reductase inhibitor simvastatin activates the protein kinase Akt and promotes angiogenesis in normocholesterolemic animals. *Nat Med.* 2000;6:1004–1010.
35. Feron O, Dessy C, Desager JP, Balligand JL. Hydroxy-methylglutaryl-coenzyme A reductase inhibition promotes endothelial nitric oxide synthase activation through a decrease in caveolin abundance. *Circulation.* 2001;103:113–118.
36. Kalinowski L, Dobrucki LW, Brovkovych V, Malinski T. Increase nitric oxide bioavailability in endothelial cells contributes to the pleiotropic effect of cerivastatin. *Circulation.* 2002;105:933–938.
37. Kondo M, Terada M, Fujiwara T, Arita N, Yano A, Tabei R. Noradrenergic hyperinnervation in the heart of stroke-prone spontaneously hypertensive rats. *Clin Exp Pharmacol Physiol Suppl.* 1995;22:S75–S76.
38. Cilla DD, Whitefield LR, Gibson DM, Sedman AJ, Posvar EL. Multiple-dose pharmacodynamics, and safety of atorvastatin, an inhibitor of HMG-CoA reductase, in healthy subjects. *Clin Pharmacol Ther.* 1996;60:687–695.
39. Moonis M, Kane K, Schwiderski U, Sandage BW, Fisher M. HMG-CoA reductase inhibitors improve acute ischemic stroke outcome. *Stroke.* 2005;36:1298–1300.
40. Sironi L, Gianazza E, Gelosa P, Guerrini U, Nobili E, Gianella A, Cremonesi B, Paoletti R, Tremoli E. Rosuvastatin, but not simvastatin, provides end-organ protection in stroke-prone rats by anti-inflammatory effects. *Arterioscler Thromb Vasc Biol.* 2005;25:598–603.

41. Di Napoli P, Antonio Taccardi A, Grilli A, Spina R, Felaco M, Barsotti A, De Caterina R. Simvastatin reduces reperfusion injury by modulating nitric oxide synthase expression: An ex vivo study in isolated working rat hearts. *Cardiovasc Res.* 2001;51:283–293.
42. Landmesser U, Engberding N, Bahlmann F, Schaefer A, Wiencke A, Heineke A, Spiekermann S, Hilfiker-Kleiner D, Templin C, Kotlarz D, Mueller M, Hornig B, Haller H, Drexler H. Statin-induced improvement of endothelial progenitor cell mobilization, myocardial neovascularization, LV function, and survival after experimental myocardial infarction requires endothelial nitric oxide synthase. *Circulation.* 2004;110:1933–1939.

Cardiovascular Research Advance Access published January 22, 2008

Cardiovascular Research
doi:10.1093/cvr/cvm092

Modulation of the myocardial redox state by vagal nerve stimulation after experimental myocardial infarction

Takaki Tsutsumi[1], Tomomi Ide[1]*, Mayumi Yamato[2], Wataru Kudou[2], Makoto Andou[1], Yoshitaka Hirooka[1], Hideo Utsumi[3], Hiroyuki Tsutsui[4], and Kenji Sunagawa[1]

[1]Department of Cardiovascular Medicine, Graduate School of Medical Sciences, Kyushu University, 3-1-1 Maidashi, Higashi-ku, Fukuoka 812-8582, Japan; [2]Department of REDOX Medicinal Science, Graduate School of Pharmaceutical Sciences, Kyushu University, Fukuoka, Japan; [3]Laboratory of Bio-function Analysis, Graduate School of Pharmaceutical Sciences, Kyushu University, Fukuoka, Japan; and [4]Cardiovascular Medicine, Hokkaido University Graduate School of Medicine, Sapporo, Japan

Received 16 July 2007; revised 24 November 2007; accepted 30 November 2007

Time for primary review: 13 days

KEYWORDS
Autonomic nervous system;
Acetylcholine;
Heart failure;
Oxidative stress

Aims Redox alteration plays a major role in the pathogenesis of heart failure (HF). Since vagal nerve stimulation (VNS) is known to improve survival and attenuate cardiac remodelling, we hypothesized that VNS may modulate the myocardial redox state.

Methods and results Using a chronic HF mouse model, we applied VNS for 15 min and measured myocardial redox status using *in vivo* electron spin resonance spectroscopy. Signal decay rate of the nitroxyl probe, an index of redox status, was enhanced in HF compared with sham (0.16 ± 0.01 vs. 0.13 ± 0.01 min^{-1}, $P < 0.05$; $n = 6$), and VNS normalized this enhancement (0.13 ± 0.01 min^{-1}, $P < 0.05$). Atropine sulphate abolished the VNS effects, indicating that the VNS modulates myocardial redox state via muscarinic receptors. N_{ω}-Nitro-L-arginine methyl ester treatment and fixed-rate atrial pacing showed a trend to suppress the VNS effects, suggesting the involvement of nitric oxide-based signalling and myocardial oxygen consumption. Moreover, VNS decreased the myocardial norepinephrine (NE) level (0.25 ± 0.07 vs. 0.60 ± 0.12 ng/mL, $P < 0.05$; $n = 6$). Reactive oxygen species production from cultured cardiomyocytes was enhanced by β-adrenergic activation, which was partially antagonized by 10 μmol/L acetylcholine (ACh) (relative value compared with control: NE 3.7 ± 0.5, NE + ACh 2.5 ± 0.3, $P < 0.05$; $n = 12$).

Conclusion The present study suggests that VNS modulates the cardiac redox status and adrenergic drive, and thereby suppresses free radical generation in the failing heart.

1. Introduction

Accumulating evidence has revealed an intimate link between the imbalance of autonomic nervous system and the pathogenesis of chronic heart failure (CHF).[1] Suppressed vagal tone and over-activated sympathetic drive accelerate cardiac remodelling and increase the risk of life-threatening tachyarrhythmia.[2] Although beta-blocker therapy aiming to antagonize the adrenergic drive is a standard treatment for CHF, the prognosis remains poor.[3]

Extensive studies and evidence have demonstrated an excessive generation of reactive oxygen species (ROS) in the failing hearts.[4–6] ROS are implicated in several pathways in CHF, such as the rennin–angiotensin–aldosterone system[7] and beta-adrenergic pathways.[8] ROS have also been proposed to alter gene expression, induce Ca^{2+} overload,[9] and activate apoptosis cascades in cardiomyocytes.[10] Furthermore, we have reported that reducing ROS by overexpressing antioxidant enzymes attenuates cardiac remodelling.[11]

Recently, Li *et al.*[12] have demonstrated that electrical stimulation of vagal nerve in post-myocardial infarction (MI)-induced CHF rats attenuates cardiac remodelling and markedly improves the prognosis, suggesting that active correction of the autonomic nervous imbalance may be a new therapeutic strategy. However, the precise mechanisms of the anti-remodelling effect of vagal nerve stimulation (VNS) have not been elucidated. It is well known that vagal nerve suppresses not only the cardiac function[13] but also cardiac sympathetic activity.[14] Moreover, electrical stimulation of cardiac parasympathetic nerve was reported to attenuate norepinephrine (NE) spillover in the left ventricle (LV), especially in the CHF animal.[15,16]

In this study, therefore, we proposed the following hypotheses: first, VNS attenuates the generation of ROS in

* Corresponding author. Tel: +81 92 642 5360; fax: +81 92 642 5374.
E-mail address: tomomi_i @cardiol.med.kyushu-u.ac.jp

the failing hearts. Secondly, redox regulation is mediated by both a decrease of cardiac NE spillover through attenuation of the cardiac sympathetic drives and a direct effect of acetylcholine (ACh) on the LV. Thirdly, NADPH oxidase is involved in the redox modulation by VNS. We tested these hypotheses *in vivo* using a murine model of CHF and *in vitro* using cultured neonatal rat cardiomyocytes.

Conventionally, it has been difficult to determine the free radical reactions or redox status *in vivo*, because free radicals and oxidants are unstable and highly reactive. The development of low frequency electron spin resonance (ESR) spectroscopy has allowed direct detection of free radicals[17] and direct estimation of the redox status in living animals non-invasively.[18] The advent of this technique has permitted the assessment of the contribution of free radicals in various pathological conditions.[19] In this study, we used *in vivo* ESR spectroscopy to evaluate a cardiac redox alteration following VNS.

We herein demonstrated for the first time that short VNS modulates the cardiac redox status and adrenergic drive, and thereby suppresses free radical generation in the failing heart.

2. Methods

2.1 Animal model of heart failure

All procedures and animal care were approved by the Committee on Ethics of Animal Experiment, Kyushu University Graduate School of Medical and Pharmaceutical Sciences and performed in accordance with the Guideline for Animal Experiment of Kyushu University, and the *Guide for the Care and Use of Laboratory Animals* published by the US National Institutes of Health (NIH Publication No. 85-23, revised 1996).

We used a murine model of CHF 28 days after induction of MI. The surgical procedure was described previously.[11] Briefly, 8–10 week-old male CD-1 mice weighing 30–35 g were used. Under anaesthesia with pentobarbital sodium (30 μg/g BW, i.p.), experimental MI was induced by ligating the left coronary artery. Control mice received sham operation without coronary artery ligation. Mice were housed in a temperature- and humidity-controlled room and fed a commercial diet and provided water *ad libitum*.

2.2 Echocardiographic and haemodynamic measurements

CHF ($n = 12$) and sham mice ($n = 12$) underwent physiological evaluation by echocardiography and left heart catheterization as previously reported.[11] Under light anaesthesia with tribromoethanol-amylene hydrate (2% Avertin, 8 μL/g BW, i.p.), two-dimensional targeted M-mode images were obtained from the short-axis view at the level of greatest LV dimension using a 7.5-MHz transducer connected to a dedicated ultrasonographic system (SSD-5500, ALOKA Co. Ltd., Tokyo, Japan). After echocardiography, a 1.4-F micromanometer-tipped catheter (Millar Instruments, Inc. Houston, TX, USA) was inserted into the right carotid artery and advanced into the LV for pressure measurement. Thereafter, mice were euthanized with overdose pentobarbital sodium. Heart and lungs were quickly excised and weighed.

2.3 Vagal nerve stimulation

CHF or control mice were randomly assigned to VNS ($n = 6$) and sham-stimulation (SS) group ($n = 6$). Under anaesthesia with pentobarbital sodium (30 μg/g BW, i.p.), the right vagal nerve was attached with a pair of stainless wire electrodes (Bioflex wire AS633; Cooner wire, Chatsworth, CA, USA) and covered with silicone

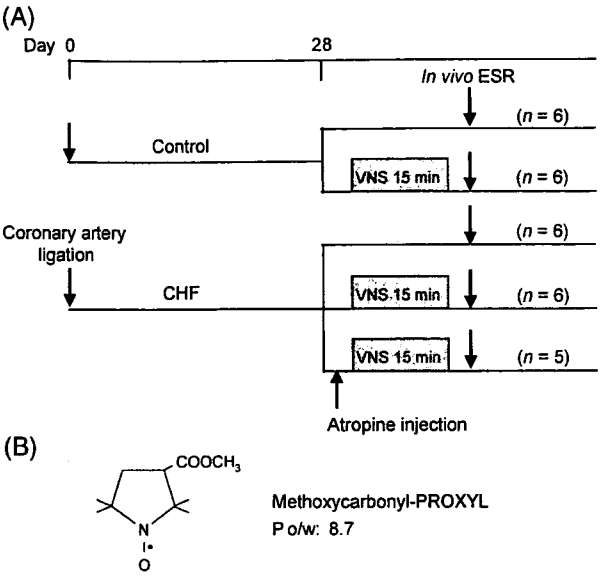

Figure 1 (*A*) Protocol scheme of the *in vivo* study in mice. Mice that survived 28 days after experimental myocardial infarction were used as a model of chronic heart failure (CHF). In CHF and sham operated control mice, sham or vagal nerve stimulation was conducted. After stimulation, methoxycarbonyl-PROXYL was injected and thereafter *in vivo* electron spin resonance (ESR) spectroscopy was performed. (*B*) Structure of methoxycarbonyl-PROXYL, a lipophilic nitroxide probe (oil : water ratio = 8.7).

gel for insulation and immobilization. The vagal nerve was stimulated with 10 Hz rectangular pulses of 1 ms duration for 15 min. Electrical voltage was optimized for each mouse so that the heart rate (HR) was reduced by 10% from baseline. In SS group, wire electrodes were implanted but VNS was not applied. Five minutes after VNS, mice subsequently underwent *in vivo* ESR analysis as described below. In a separate series of experiments, CHF mice were given intravenous injection of atropine sulphate (1 μg/g BW, Sigma-Aldrich, Inc., St Louis, MO, USA), followed by VNS, rectangular pulses of which were 10 Hz, and duration is 1 ms (*Figure 1A*). Electrical voltage was fixed at 500 mV, because muscarinic blockade abolishes the VNS induced HR reduction, and this electrical condition could reduce HR in almost all CHF and control mice.

In another series of experiments, we performed fixed rate atrial pacing during VNS to determine the impact of bradycardia. In brief, after implantation of electrical wires, the left chest was opened under artificial ventilation. A pair of stainless wires was surgically attached with left atrium. After HR reached constant, VNS and fixed rate atrial pacing were simultaneously initiated. The vagal nerve was stimulated with rectangular pulses of 1-ms duration, 10 Hz, 500 mV for 15 min. Rectangular pulses for atrial pacing were also of 1-ms duration. After 15 min of VNS and atrial pacing, the chest was closed and mice subsequently underwent *in vivo* ESR.

To elucidate the role of nitric oxide (NO) pathway, we applied VNS in mice treated with N_ω-nitro-L-arginine methyl ester (L-NAME) hydrochloride (Sigma-Aldrich). L-NAME (1 mg/kg/day) was administered to CHF mice through drinking water for 7 days prior to the experiment. The condition of VNS was same as in CHF + VNS mice.

2.4 *In vivo* electron spin resonance spectroscopy

We performed *in vivo* ESR spectroscopy to assess the myocardial redox state. This method is based on the theory that nitroxyl radicals are reduced to the corresponding hydroxylamine in the presence of free radicals *in vivo*, resulting in the disappearance of ESR signals.[18] A semilogarithmic plot of time course of the ESR signals shows a linear decay curve, the rate of which (a reciprocal

number of time constant) is proportional to the amount of reductants including free radicals. Prior to *in vivo* ESR analysis, mice were given intravenous injection of 3-methoxycarbonyl-2,2,5,5,5-tetramethylpyrrolidine-l-oxyl (methoxycarbonyl-PROXYL) (0.3 μmol/L/g BW), a membrane permeable nitroxyl spin probe (oil : water ratio = 8.7) (*Figure 1B*), which was synthesized as described previously.[20] Shortly thereafter, ESR spectra were recorded at regular intervals at chest region using L-band ESR spectrometer (JEOL Co. Ltd., Akishima, Japan) with a loop-gap resonator (33 mm i.d. and 30 mm in length). The power of the 1.1 GHz microwave was 1.67 mW.

First, as a validation study, we performed *in vivo* ESR in control and CHF mice, to which VNS were not applied, to determine whether the difference in signal decay could be observed between these mice. Secondly, we assessed the effect of two ROS scavengers, 1,2-dihydroxy-3,5-benzenedisulphonic acid disodium salt monohydrate (tiron) (10 μmol/mouse, Dojindo Molecular Lanoratories Co. Ltd., Kumamoto, Japan) and dimethylthiourea (DMTU) (10 μmol/mouse, Sigma-Aldrich), on ESR signal decay. These chemicals were administered intravenously prior to methoxycarbonyl-PROXYL injection. Thirdly, we performed *in vivo* ESR in CHF and control mice after VNS or SS.

2.5 Cardiac level of low molecular weight thiols

Cardiac level of low molecular weight thiols, which is mainly reduced glutathione (GSH), was measured by the 5,5′-dithiobis(2-nitrobenzoic acid) (DTNB) method. After sham or vagal stimulation for 15 min ($n = 6$ each), CHF mice were euthanized and hearts were quickly excised. Non-infarcted LV was homogenized with 4% sulphosalicylic acid and 10 μL of supernatant was incubated with 125 μL of 1.5 mmol/L DTNB at 37°C for 15 min. Absorbance at 405 nm was measured. Thiol concentration was determined by calibration using 0–2 mmol/L GSH, and was expressed as μmol/L/mg tissue.

2.6 Cytochrome *c* reduction assay

NADPH oxidase activity was examined using superoxide dismutase inhibitable cytochrome *c* reduction assay. After sham or vagal stimulation for 15 min, mice were euthanized and the heart was quickly excised. Non-infarcted LV sample was immediately homogenized with phosphate buffer saline. Ten μL of the supernatants (final concentration 3 mg/mL) were diluted in 190 μL of assay buffer (300 mmol/L potassium phosphate, 0.1 mmol/L EDTA, 36 μmol/L cytochrome *c*, pH 7.8) in 96-well plates. NADPH (1 μmol/L) was added in the presence or absence of SOD (200 U/mL). Cytochrome *c* reduction was measured by reading the absorbance at 550 nm on microplate reader. NADPH oxidase activity was calculated from the difference between the absorbance with or without SOD and the extinction coefficient (21.1 mmol/L/cm) for reduced cytochrome *c*. Cytochrome *c* reductase positive control (Sigma-Aldrich) was used to verify the specificity of the assay. Results were expressed as unit/mL, which was defined as reduction in 1.0 μmol of oxidized cytochrome *c* in the presence of 100 μmol/L NADPH per minute at pH 7.8 at 25°C.

2.7 Cardiac level of norepinephrine

Cardiac level of NE was measured by microdialysis and high performance liquid chromatography (HPLC). We used a transverse dialysis probe consisted of a dialysis fibre (2 mm in length, 220 μm in outer diameter, 200 μm in inner diameter, molecular weight cutoff at 50 kDa; OP-50-2, Eikom, Kyoto, Japan). Under light anaesthesia with pentobarbital sodium (20 μg/g BW, i.p.), mice were mechanically ventilated. After implantation of electrical wires, the left chest was opened. A dialysis probe was implanted into the non-infarcted LV. Ringer's solution (Na^+; 147 mmol/L, K^+; 4 mmol/L, Ca^{2+}; 1.26 mmol/L, Mg^{2+}; 1 mmol/L, Cl^-; 155.6 mmol/L) was pumped at a constant flow rate of 2 μL/min. Microdialysis session was started after a 30-min equilibration period. After collecting pre-VNS (baseline) samples for 30 min, VNS was started. From 15 min after VNS initiation, VNS samples were collected for 30 min. Finally, post-VNS samples were collected 15 min after the termination of VNS. NE concentration was assayed by HPLC, the condition of which was described in Supplementary Method.

2.8 Reactive oxygen species production in cultured neonatal rat ventricular cardiomyocytes

Primary cultures of cardiomyocytes were prepared from the ventricles of neonatal Wistar rats as described previously.[21] Briefly, after digestion of the myocardial tissue with trypsin, cells were suspended in Dulbecco's Modified Eagle's Medium (Sigma-Aldrich) containing 10% FBS and preplated twice in 100-mm culture dishes for 70 min each to reduce the number of non-myocytes. Non-adherent cells were plated in 12-well cultured plates at a density of 10^3 cells per mm^2. Cardiomyocytes were maintained at 37°C in humidified air with 5% CO_2. The culture medium was replaced by Hanks' balanced salt solution with Ca^{2+} and Mg^{2+} but without phenol red (Gibco, Invitrogen, Carlsbad, CA, USA) 24 h before the experiments.

On culture day 4, cells were exposed to NE (Sigma-Aldrich) in concentration from 0.01 to 100 μmol/L under the simultaneous incubation with prazosin hydrochloride (0.1 μmol/L) (Sigma-Aldrich) for 30 min to determine the ROS production from cardiomyocytes in response to β-adrenergic activation. H_2O_2 concentration in the culture medium was measured as described below. In a separate series of experiments, to elucidate the effect of ACh on the ROS production via β-adrenergic activation, cells were incubated with NE (10 μmol/L), NE + ACh (10 μmol/L) (Sigma-Aldrich), and NE + ACh + atropine hydrochloride (10 μmol/L) (Sigma-Aldrich). All NE-treated cells were incubated with 0.1 μmol/L prazosin. ACh and atropine were added 30 min prior to NE exposure. In the experiment to elucidate the ROS production within the myocytes, cells were incubated with 5 μmol/L of 2′,7′-dichlorofluorescin diacetate (DCFH-DA) (Sigma-Aldrich) at 37°C for 30 min. The fluorescence images were acquired with a microscope (BX50, Olympus Co. Ltd., Tokyo, Japan). Relative intensity for treated cells was determined by comparing with control cells. The experiment was repeated three times independently. For an experiment to determine the extracellular ROS production, after incubation at 37°C for 30 min, we collected the conditioned culture medium.

The H_2O_2 concentration was measured by the method reported by Keston and Brandt.[22] In brief, 10 μL of sample ($n = 10$ each) was reacted *in vitro* with 1 μmol/L DCFH-DA. Oxidation of DCFH-DA to the fluorescent 2-7-dichlorofluorescein (DCF) by H_2O_2 was investigated by measuring fluorescence at an excitation wavelength of 510 nm and an emission wavelength of 550 nm. The fluorescence intensity was corrected by subtracting the value of the sample treated with catalase. The concentration of H_2O_2 was determined by calibration using 0–10 μmol/L H_2O_2.

2.9 Statistical analysis

Data are presented as mean ± SEM. Significant differences were determined by one-way analysis of variance using the Tukey post hoc test. Myocardial NE concentrations before and during VNS were compared by a paired *t*-test, after confirming normal distribution. A *P*-value less than 0.05 was judged to represent a statistically significant difference.

3. Results

3.1 Animal characteristics

LV dimensions were significantly enlarged and systolic function was significantly reduced in CHF, compared with control mice (*Table 1*). Although there was no significant difference in HR, the values of mean aortic pressure, LV + d*p*/d*t* max

and $-dp/dt$ max were lower, and LV end-diastolic pressure was higher in CHF than in control. Heart weight/body weight, LV weight/body weight, and lung weight have also increased in CHF. Four mice out of 12 had obvious pleural effusion, whereas no effusion was present in control mice.

Table 1 Characteristics of the chronic heart failure (CHF) mouse model

	Control ($n = 12$)	CHF ($n = 12$)
Body weight (g)	40.0 ± 0.5	39.1 ± 0.8
Echocardiographic data		
Heart rate (bpm)	539 ± 13	535 ± 27
LVEDD (mm)	3.6 ± 0.1	5.9 ± 0.2*
LVESD (mm)	2.1 ± 0.3	5.5 ± 0.3*
FS (%)	42.9 ± 1.0	6.8 ± 0.9*
Haemodynamic data		
Mean AoP (mmHg)	89 ± 3	76 ± 4*
LVEDP (mmHg)	2.5 ± 0.2	16.6 ± 1.7*
+ dp/dt max (mmHg/s)	12900 ± 400	4900 ± 400*
− dp/dt max (mmHg/s)	−8600 ± 300	−3300 ± 200*
Organ weight data		
Heart wt/body wt (mg/g)	4.9 ± 0.1	10.8 ± 0.3*
LV wt/body wt (mg/g)	3.0 ± 0.1	4.0 ± 0.1*
Lung weight (mg)	183 ± 4	366 ± 20*

LV, left ventricular; EDD, end-diastolic diameter; ESD, end-systolic diameter; FS, fractional shortening; AoP, aortic pressure; EDP, end-diastolic pressure; wt, weight. Values are mean ± SEM.
$^{*}P < 0.05$ and $^{*}P < 0.01$ vs. control.

3.2 Measurement of reactive oxygen species by *in vivo* electron spin resonance

The signal decay rate of methoxycarbonyl-PROXYL at the chest region in CHF mice was clearly enhanced compared with controls (*Figure 2A*). This increased signal decay rate was almost reversed by the treatment with tiron or DMTU (*Figure 2B*), suggesting that the total redox state was changed probably due to increased ROS production especially in the failing myocardium.

In the next VNS protocol, VNS elicited a similar HR reduction in both CHF and control mice. Although there were some minor differences in each animal, from 300 to 500 mV were needed to reduce HR by 10% from baseline. No HR reduction by electrical stimulation (500 mV) was observed in CHF mice treated with atropine. *In vivo* ESR spectroscopy revealed that VNS normalized the enhanced signal decay in CHF mice. In control mice, VNS showed no effects on the signal decay rate. Furthermore, this vagal-mediated effect in CHF mice was abolished by the administration of atropine (*Figure 2C*). These results suggested that VNS normalized the altered redox state in the failing myocardium potentially through attenuating the overproduction of ROS via muscarinic ACh receptor pathway.

As an additional series of experiments, we performed *in vivo* ESR in CHF mice under fixed rate atrial pacing to exclude the effects of bradycardia. Fixed rate pacing showed a trend to abolish the VNS effects (*Figure 3A*).

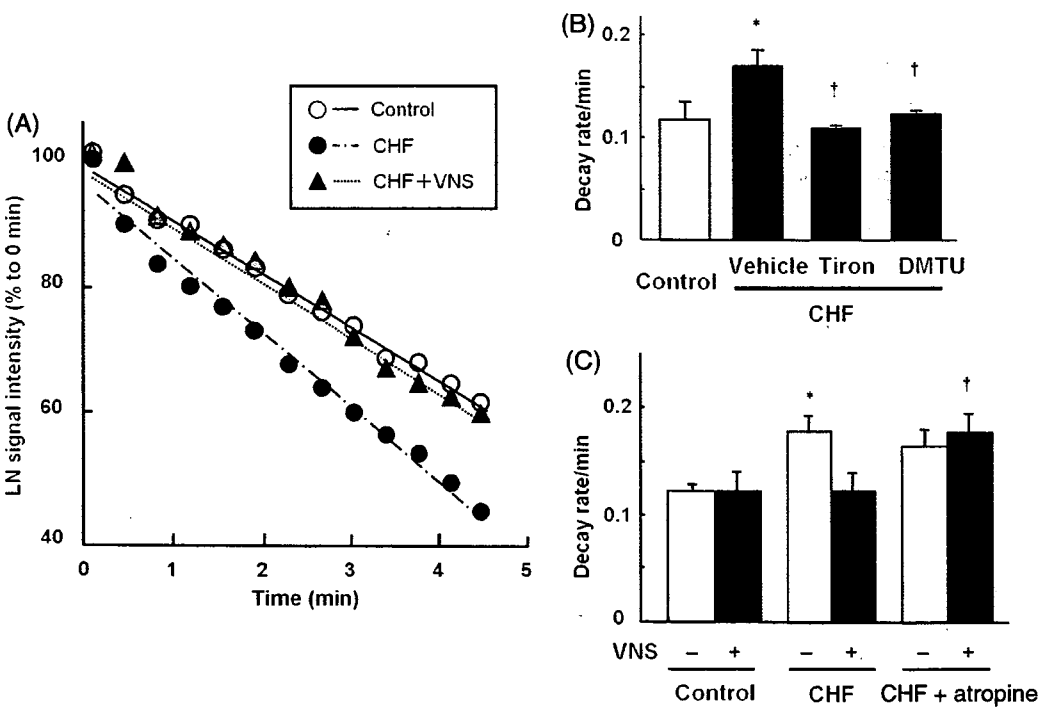

Figure 2 Effects of vagal nerve stimulation (VNS) on the signal decay of methoxycarbonyl-PROXYL at the chest region in control and chronic heart failure (CHF) mice with or without VNS. The electron spin resonance (ESR) signal decay curve was obtained by plotting the peak height of the ESR signals semilogarithmically as a function of time. (*A*) Typical *in vivo* ESR signal decay curves of methoxycarbonyl-PROXYL in control mouse (○), CHF mouse without VNS (●) and CHF mouse with VNS (?). Solid and broken lines are linear fits to the respective data. (*B*) Signal decay rates (calculated from the slopes of fitted lines) in CHF mice administered vehicle or the antioxidant tiron (400 μmol/kg) or DMTU (400 μmol/kg). $^{*}P < 0.05$ vs. control; $\dagger P < 0.05$ vs. CHF-vehicle, $n = 6$ in each group. (*C*) Signal decay rates in mice of control, CHF and CHF with atropine administration. $^{*}P < 0.05$ vs. control without VNS; $\dagger P < 0.05$ vs. CHF with VNS, $n = 5$ in CHF with atropine administration group, $n = 6$ in other groups. The data in B and C are presented as means ± SEM.

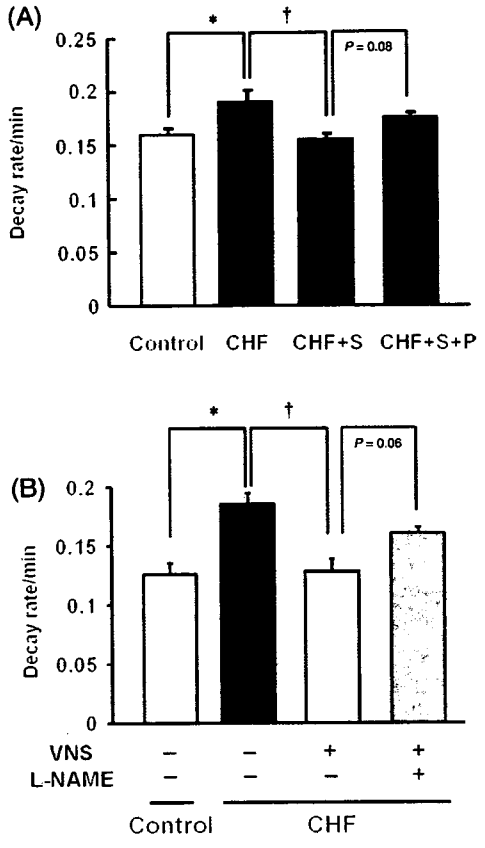

Figure 3 (*A*) *In vivo* electron spin resonance signal decay rates in mice of control, chronic heart failure (CHF), CHF + vagal nerve stimulation (VNS) (CHF + S), and CHF + VNS under fixed rate pacing (CHF + S + P). $^{*}P < 0.05$ vs. control; $^{\dagger}P < 0.05$ vs. CHF, *P*-value between CHF + S and CHF + S + P was 0.08. $n = 7$ in group of control and CHF, $n = 5$ in group of CHF + S and CHF + S + P. (*B*) Signal decay rates in mice of control, CHF, CHF + VNS, and CHF + VNS with N_{ω}-nitro-L-arginine methyl ester (L-NAME) (1 mg/kg/day). L-NAME treatment showed a tendency for attenuating the VNS induced antioxidative effects ($P = 0.062$ vs. CHF + VNS). $^{*}P < 0.05$ vs. control; $^{\dagger}P < 0.05$ vs. CHF, $n = 7$ in group of control and CHF, $n = 6$ in group of CHF + VNS and CHF + VNS + L-NAME. The data are presented as means ± SEM.

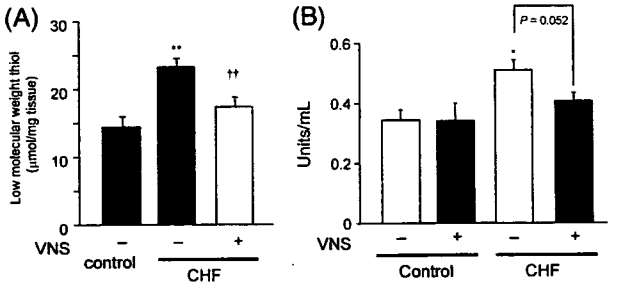

Figure 4 (*A*) Effects of vagal nerve stimulation (VNS) on cardiac concentration of low molecular thiols. The values are means ± SEM, $n = 6$ in each group. $^{**}P < 0.01$ vs. control without VNS; $^{\dagger\dagger}P < 0.01$ vs. chronic heart failure (CHF) without VNS. (*B*) Myocardial NADPH oxidase activity. $^{*}P < 0.05$ vs. control without VNS. $n = 6$ in each group.

Furthermore, we also performed *in vivo* ESR analysis in CHF mice treated with L-NAME to clarify the involvement of NO. L-NAME treated mice showed a diminished HR response to VNS and a tendency to reduce the VNS induced improvements in myocardial redox state (*Figure 3B*).

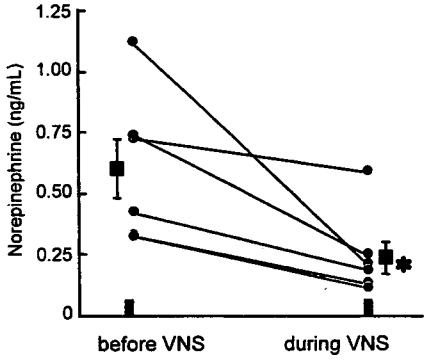

Figure 5 Cardiac norepinephrine levels with or without vagal nerve stimulation (VNS), assessed by microdialysis and high performance liquid chromatography. Closed circles and lines indicate the level of norepinephrine before and during VNS in each animal. Squares and error bars indicate means ± SEM, $n = 6$ in each group. $^{*}P < 0.05$ vs. before VNS.

3.3 Cardiac concentration of low molecular weight thiols

The myocardial concentration of low molecular weight thiols was significantly increased in CHF compared with control mice, and the increase was significantly attenuated by 15-min VNS (*Figure 4A*). This result also supported the observation that the redox status in the failing myocardium was altered by short application of VNS.

3.4 Nicotinamide adenin dinucleotide phosphate (NADPH) oxidase activity

Western blot analysis and cytochrome *c* reduction assay were performed on LV samples taken from control or CHF mice after the VNS or SS. Although the myocardial expression of $p47^{phox}$, a cytosolic subunit of NADPH oxidase, was significantly increased in CHF mice, it was not altered after VNS (see Supplementary Methods and Supplementary material online, *Figure S1A and B*). Cytochrome *c* reduction assay revealed that myocardial NADPH oxidase activity was enhanced in CHF mice relative to control mice (0.51 ± 0.02 units/mL CHF + SS vs. 0.34 ± 0.03 units/mL control + SS, $P < 0.05$) and that there was a tendency for a reduction in NADPH oxidase acitivity by VNS (0.40 ± 0.03 units/mL CHF + VNS, $P = 0.052$) (*Figure 4B*).

3.5 Cardiac norepinephrine concentration

Cardiac NE concentration in CHF mice decreased significantly during VNS compared with before VNS (0.25 ± 0.07 ng/mL during VNS vs. 0.61 ± 0.12 ng/mL before VNS, $P < 0.05$) (*Figure 5*) and returned to baseline after the termination of VNS (0.43 ± 0.07 ng/mL after VNS vs. 0.25 ± 0.07 ng/mL during VNS, $P < 0.05$). Although it did not reach statistical significance, VNS induced reduction in NE level was also observed in control mice (0.47 ± 0.06 ng/mL before VNS, 0.36 ± 0.08 ng/mL during VNS, 0.42 ± 0.02 ng/mL after VNS, $P > 0.05$). These results suggested that VNS inhibited sympathetic nerve presynaptically especially in CHF mice.

3.6 β-Adrenergic receptor mediated reactive oxygen species production in cardiomyocytes

An increase in DCF fluorescence was observed 30 min after β-adrenergic receptor (β-AR) stimulation of cultured cardiomyocytes with 10 μmol/L NE. Furthermore, NE also increased the extracellular H_2O_2 release in a concentration-dependent manner (*Figure 6A*), confirming that β-AR stimulation increased the production of ROS in cardiomyocytes. The NE-induced DCFH oxidation was inhibited significantly by the addition of 10 μmol/L ACh, and this effect was abolished by atropine sulphate (*Figure 6B*), indicating that ACh directly inhibits the β-AR-stimulated ROS production in cardiomyocytes. The anti-oxidative effect of ACh was also demonstrated in NE-induced extracellular H_2O_2 release. ACh partially but significantly attenuated the NE-induced H_2O_2 release (46% reduction), which was also abolished by the addition of atropine sulphate (*Figure 6C*).

4. Discussion

The major findings demonstrated in the present study are that: (i) short VNS altered the myocardial redox status in CHF mice; (ii) this observation was mediated by both an inhibition of sympathetic drive and a direct action of ACh against free radical generation in the myocardium; and (iii) the subcellular mechanisms may involve NADPH oxidase activation, NO production, and myocardial oxygen consumption.

Cardiac parasympathetic nerve may play a defensive role in the pathogenesis of various heart diseases. According to the previous studies, VNS not only reduces the occurrence of lethal ventricular tachyarrhythmia[23,24] but also attenuates the development of cardiac remodelling.[12] In addition to these effects, the present study demonstrated that VNS suppresses myocardial ROS over-production. ROS cause cardiac apoptosis and activate several maladaptive cascades, which in turn lead to further dysfunction of cardiomyocytes.[10] Therefore, the vagal-mediated anti-oxidative effects in the failing heart may provide an important mechanism contributing to the anti-remodelling action of chronic VNS.

4.1 Alteration of myocardial redox state by vagal nerve stimulation

We used *in vivo* ESR spectroscopy with a spin probe to measure the excess amount of ROS generation or estimate the redox status in living animals.[18] CHF mice with marked LV systolic dysfunction showed enhanced ESR signal decay compared with controls. The increased signal decay rate in CHF mice indicates alteration of the redox status, probably due to excess ROS generation, because administration of antioxidants normalized the accelerated signal decay. Strikingly, the enhanced signal decay was almost normalized by

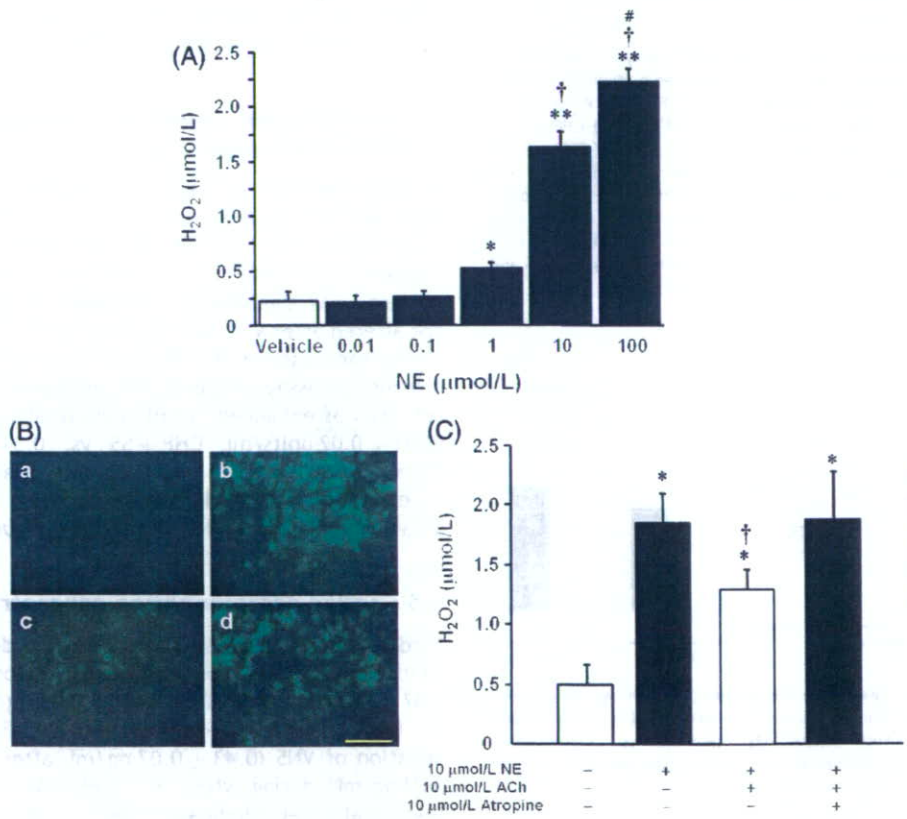

Figure 6 *In vitro* effects of acetylcholine (ACh) on norepinephrine (NE)-induced oxidants production in cardiomyocytes. (*A*) NE induced extracellular H_2O_2 release in a concentration-dependent manner. Values are means ± SEM, $n = 12$ in each group. $^*P < 0.05$ and $^{**}P < 0.01$ vs. vehicle; $^{\dagger}P < 0.05$ vs. 1 μmol/L NE; $^{\#}P < 0.05$ vs. 10 μmol/L NE. (*B*) Dichlorofluorescein fluorescence within cardiomyocytes. Cells were incubated with vehicle (a), 10 μmol/L NE (b), 10 μmol/L NE with 10 μmol/L ACh (c), 10 μmol/L NE with 10 μmol/L ACh in the presence of 10 μmol/L atropine (d). (*C*) Suppression of NE-induced extracellular H_2O_2 release by ACh. Values are means ± SEM, $n = 10$ in each group. $^*P < 0.05$ vs. vehicle; $^{\dagger}P < 0.05$ vs. 10 μmol/L NE.

15-min VNS, which was not observed in control mice. Therefore, these results indicated that a short VNS suppressed the enhanced ROS generation especially in the failing heart. Furthermore, the VNS-induced effects are mediated by muscarinic ACh receptors, because administration of atropine sulphate blocked the VNS-induced effects. Moreover, the cardiac level of low molecular weight thiols, which was mainly reduced form of GSH, was altered in parallel with the ESR signal decay as a result of VNS, suggesting modulation in myocardial redox state. However, the increased GSH in the failing myocardium is in contrast to the previous reports.[25,26] These controversial findings may be due to contribution of various factors, including experimental conditions and animal species employed, namely the difference in HF models, details of which are unknown at the moment.

4.2 Antioxidant effects by inhibition of norepinephrine and release of acetylcholine

Regarding autonomic innervation in the heart, previous studies both in animals and in humans have demonstrated that NE released by cardiac sympathetic nerve can be suppressed by parasympathetic activation via muscarinic receptor located at adrenergic nerve terminals.[14] This effect is more prominent especially under a condition of enhanced adrenergic drive.[15,16] Furthermore, the high concentration of NE is cardiotoxic[27] and induces apoptosis,[8] playing a central role at the formation of a vicious cycle in the pathogenesis of HF. In this study, VNS decreased the cardiac NE level *in vivo*, suggesting sympathetic inhibition. In addition, in cardiomyocytes, NE generated ROS in a concentration-dependent manner. Taken together, sympatho-inhibition may be one mechanism of vagally mediated antioxidative effects in the failing heart.

It is well known that ACh released from vagal terminals also counteracts AR signalling within cardiomyocytes. Adenylylcyclase which is activated by Gs protein coupled with β-AR is inhibited by pertussis toxin-sensitive Gi/o protein coupled with M2 muscarinic receptor.[28] VNS increases the interstitial ACh level in the heart.[29] In this study, β-adrenoceptor-mediated ROS production in cardiomyocytes was suppressed by the co-incubation with ACh. Therefore, the increased interstitial ACh evoked by VNS may also protect heart from oxidative stress *in vivo*. However, since NE-induced ROS production was partially inhibited by ACh, the direct effect of ACh does not fully explain our *in vivo* ESR results, indicating that other mechanisms may intervene between the anti-oxidative effects and VNS.

4.3 Involvement of nitric oxide and NADPH oxidase

One potential mechanism is the involvement of NO. It is well established that NO and NO-based signal transduction pathways modulate myocardial physiological function.[30] Altered production of reactive oxygen and nitrogen species, which is defined as redox disequilibrium, is one of the major characteristics of failing myocardium.[30] Indeed, *in vivo* ESR spectroscopy in our study revealed that chronic treatment with L-NAME attenuated the VNS-induced effects. Therefore, NO may mediate the normalization of myocardial redox disequilibrium by VNS. Dedkova *et al.*[31] demonstrated that ACh increases NO production in cardiomyocytes. NO itself may act as a ROS scavenger at low physiologic levels.[32] Furthermore, possible involvement of neuronal NO synthase should be taken into consideration. Extensive studies by Mohan and colleagues[33] have shown that neuronal NO facilitates vagal neurotransmission and bradycardia via cGMP-dependent pathway. We also observed diminished HR response to VNS in CHF mice treated with L-NAME. Although we could not speculate to what extent myocardial or neuronal NO production contributes, NO and NO-based signal transduction pathways play important roles in the VNS induced myocardial redox modulation.

Among the several myocardial sources of oxidative stress, NADPH oxidase has been clarified as one of the major sources in the failing myocardium. NADPH oxidase isoform Nox2, which is abundantly expressed in cardiomyocytes, is regulated by cytosolic components, $p47^{phox}$, $p67^{phox}$, $p40^{phox}$, and rac.[6] It is reported that both NADPH oxidase activity and $p47^{phox}$ expression are enhanced in the diseased myocardium not only in animal models[34] but also in humans.[35] Expression of $gp47^{phox}$ and NADPH oxidase activity were also enhanced in the LV of CHF mice. VNS did not alter the protein level of $gp47^{phox}$, whereas the enhanced NADPH oxidase activity was attenuated by VNS. This observation would confirm our result that VNS resets the myocardial redox imbalance. It is natural that enzymatic reactions or activations are involved in the acute myocardial redox modulation. Although the mechanism how VNS attenuated NADPH oxidase activity is uncertain, NO is suggested to inhibit NADPH oxidases.[36] Therefore, VNS induced NADPH oxidase regulation may also be mediated by NO.

Regarding the cardiac mechanics and energetics, decrease in HR reduces myocardial oxygen consumption.[37] This may contribute to the VNS-induced redox alteration to some extent, because fixed rate atrial pacing partially inhibited the VNS effects. There are several mechanisms to explain this partial inhibition. As previously reported, inotropic effects of VNS were influenced by the presence of sympathetic drive.[13] Without sympathetic drive, it is mainly mediated by indirect effect of bradycardia via force frequency mechanism.[37] In contrast, with sympathetic drive, inotropic effects of VNS are also mediated by direct effects which are independent of HR. Therefore, partial inhibition by atrial pacing may be attributed to the inhibition of indirect bradycardic effects. Although it is difficult to define the extent of contribution of bradycardia, reduction in myocardial oxygen consumption, at least in part, plays a role in myocardial redox modulation by VNS.

4.4 Limitations

There are several limitations and unsolved questions. First, care should be paid to interpret that the enhanced signal decay is due to the increase in ROS, because reductants such as ascorbic acid, GSH, and NO are known to reduce nitroxyl radicals *in vivo*. However, the accelerated signal decay in CHF mice was normalized by the administration of antioxidants. Therefore, it appears to be reasonable postulate that VNS suppresses ROS-overproduction and modulates the myocardial redox status in CHF mice. Secondly, we stimulated vagal nerve for 15 min and the electrical voltage was optimized to reduce HR by 10%. We did not examine details of the influence of duration or strength, which remains for future study. Thirdly, involvements of

central nervous system (CNS) and anaesthetic agents remain unknown. Inputs to CNS via vagal afferents have been reported to modulate several neuronal reflexes and the activities of autonomic nervous system.[38] Since we also observed both the presser and depressor responses to vagal afferent stimulation in rats (data not shown), alteration of CNS function may affect the present results. Furthermore, anaesthetic agents suppress autonomic nervous activity. The myocardial NE levels, therefore, might be different from that in conscious animals. Fourthly, the concentration of NE used in cultured cardiomyocyte experiments was much higher than physiological plasma NE concentration *in vivo*. Therefore, these issues, the reason of which are not clarified in the current study *in vitro*, have to be taken into consideration to explain the pathophysiological mechanism responsible for the regulation *in vivo*.

4.5 Conclusions

In conclusion, in a mouse model of chronic HF, VNS modulates the cardiac redox status and adrenergic drive thereby suppressing ROS generation in the failing heart.

Supplementary material

Supplementary material is available at *Cardiovascular Research* online.

Acknowledgements

We thank Dr Atsunori Kamiya (National Cardiovascular Centre Research Institute, Osaka, Japan) for technical advice and Ms Keiko Kurakazu for technical assistance. We appreciate the technical support from the Research Support Center, Graduate School of Medical Sciences, Kyushu University.

Conflict of interest: none declared.

Funding

This study was supported in part by grants from the Ministry of Education, Science and Culture (Nos 17790490 and 17790037), and from the Ministry of Health, Labor, and Welfare (Research Grant for Comprehensive Research in Aging and Health Labor and Welfare of Japan), Grant from Japan Cardiovascular Research Foundation, Uehara Memorial Foundation, and Mitsubishi Pharma Research Foundation. A part of this study was conducted in Kyushu University Station for Collaborative Research II.

References

1. Cohn JN, Levine TB, Olivari MT, Garberg V, Lura D, Francis GS *et al.* Plasma norepinephrine as a guide to prognosis in patients with chronic congestive heart failure. *N Engl J Med* 1984;**311**:819–823.
2. Floras JS. Clinical aspects of sympathetic activation and parasympathetic withdrawal in heart failure. *J Am Coll Cardiol* 1993;**22**:72A–84A.
3. Jessup M, Brozena S. Heart failure. *N Engl J Med* 2003;**348**:2007–2018.
4. McMurray J, Chopra M, Abdullah I, Smith WE, Dargie HJ. Evidence of oxidative stress in chronic heart failure in humans. *Eur Heart J* 1993;**14**: 1493–1498.
5. Ide T, Tsutsui H, Kinugawa S, Suematsu N, Hayashidani S, Ichikawa K *et al.* Direct evidence for increased hydroxyl radicals originating from superoxide in the failing myocardium. *Circ Res* 2000;**86**:152–157.
6. Murdoch CE, Zhang M, Cave AC, Shah AM. NADPH oxidase-dependent redox signalling in cardiac hypertrophy, remodelling and failure. *Cardiovasc Res* 2006;**71**:208–215.
7. Aikawa R, Komuro I, Yamazaki T, Zou Y, Kudoh S, Tanaka M *et al.* Oxidative stress activates extracellular signal-regulated kinases through Src and Ras in cultured cardiac myocytes of neonatal rats. *J Clin Invest* 1997; **100**:1813–1821.
8. Communal C, Singh K, Pimentel DR, Colucci WS. Norepinephrine stimulates apoptosis in adult rat ventricular myocytes by activation of the beta-adrenergic pathway. *Circulation* 1998;**98**:1329–1334.
9. Luo J, Xuan YT, Gu Y, Prabhu SD. Prolonged oxidative stress inverts the cardiac force-frequency relation: role of altered calcium handling and myofilament calcium responsiveness. *J Mol Cell Cardiol* 2006;**40**:64–75.
10. Cesselli D, Jakoniuk I, Barlucchi L, Beltrami AP, Hintze TH, Nadal-Ginard B *et al.* Oxidative stress-mediated cardiac cell death is a major determinant of ventricular dysfunction and failure in dog dilated cardiomyopathy. *Circ Res* 2001;**89**:279–286.
11. Shiomi T, Tsutsui H, Matsusaka H, Murakami K, Hayashidani S, Ikeuchi M *et al.* Overexpression of glutathione peroxidase prevents left ventricular remodeling and failure after myocardial infarction in mice. *Circulation* 2004;**109**:544–549.
12. Li M, Zheng C, Sato T, Kawada T, Sugimachi M, Sunagawa K. Vagal nerve stimulation markedly improves long-term survival after chronic heart failure in rats. *Circulation* 2004;**109**:120–124.
13. Nakayama Y, Miyano H, Shishido T, Inagaki M, Kawada T, Sugimachi M *et al.* Heart rate-independent vagal effect on end-systolic elastance of the canine left ventricle under various levels of sympathetic tone. *Circulation* 2001;**104**:2277–2279.
14. Azevedo ER, Parker JD. Parasympathetic control of cardiac sympathetic activity: normal ventricular function versus congestive heart failure. *Circulation* 1999;**100**:274–279.
15. Levy MN, Blattberg B. Effect of vagal stimulation on the overflow of norepinephrine into the coronary sinus during cardiac sympathetic nerve stimulation in the dog. *Circ Res* 1976;**38**:81–84.
16. Newton GE, Parker AB, Landzberg JS, Colucci WS, Parker JD. Muscarinic receptor modulation of basal and beta-adrenergic stimulated function of the failing human left ventricle. *J Clin Invest* 1996;**98**:2756–2763.
17. Zweier JL, Kuppusamy P. Electron paramagnetic resonance measurements of free radicals in the intact beating heart: a technique for detection and characterization of free radicals in whole biological tissues. *Proc Natl Acad Sci USA* 1988;**85**:5703–5707.
18. Utsumi H, Muto E, Masuda S, Hamada A. In vivo ESR measurement of free radicals in whole mice. *Biochem Biophys Res Commun* 1990;**172**: 1342–1348.
19. Yamato M, Egashira T, Utsumi H. Application of in vivo ESR spectroscopy to measurement of cerebrovascular ROS generation in stroke. *Free Radic Biol Med* 2003;**35**:1619–1631.
20. Sano H, Matsumoto K, Utsumi H. Synthesis and imaging of blood-brain-barrier permeable nitroxyl-probes for free radical reactions in brain of living mice. *Biochem Mol Biol Int* 1997;**42**:641–647.
21. Suematsu N, Tsutsui H, Wen J, Kang D, Ikeuchi M, Ide T *et al.* Oxidative stress mediates tumor necrosis factor-alpha-induced mitochondrial DNA damage and dysfunction in cardiac myocytes. *Circulation* 2003;**107**: 1418–1423.
22. Keston AS, Brandt R. The fluorometric analysis of ultramicro quantities of hydrogen peroxide. *Anal Biochem* 1965;**11**:1–5.
23. Vanoli E, De Ferrari GM, Stramba-Badiale M, Hull SS Jr, Foreman RD, Schwartz PJ. Vagal stimulation and prevention of sudden death in conscious dogs with a healed myocardial infarction. *Circ Res* 1991;**68**: 1471–1481.
24. Ando M, Katare RG, Kakinuma Y, Zhang D, Yamasaki F, Muramoto K *et al.* Efferent vagal nerve stimulation protects heart against ischemia-induced arrhythmias by preserving connexin43 protein. *Circulation* 2005;**112**: 164–170.
25. Hill MF, Singal PK. Right and left myocardial antioxidant responses during heart failure subsequent to myocardial infarction. *Circulation* 1997;**96**: –2414–2420.
26. Khaper N, Singal PK. Modulation of oxidative stress by a selective inhibition of angiotensin II type 1 receptors in MI rats. *J Am Coll Cardiol* 2001;**37**:1461–1466.
27. Mann DL, Kent RL, Parsons B, Cooper Gt. Adrenergic effects on the biology of the adult mammalian cardiocyte. *Circulation* 1992;**85**: 790–804.
28. Dhein S, van Koppen CJ, Brodde OE. Muscarinic receptors in the mammalian heart. *Pharmacol Res* 2001;**44**:161–182.
29. Akiyama T, Yamazaki T, Ninomiya I. In vivo detection of endogenous acetylcholine release in cat ventricles. *Am J Physiol* 1994;**266**: H854–H860.

30. Hare JM, Stamler JS. NO/redox disequilibrium in the failing heart and cardiovascular system. *J Clin Invest* 2005;115:509–517.
31. Dedkova EN, Ji X, Wang YG, Blatter LA, Lipsius SL. Signaling mechanisms that mediate nitric oxide production induced by acetylcholine exposure and withdrawal in cat atrial myocytes. *Circ Res* 2003;93:1233–1240.
32. Wink DA, Miranda KM, Espey MG, Pluta RM, Hewett SJ, Colton C *et al.* Mechanisms of the antioxidant effects of nitric oxide. *Antioxid Redox Signal* 2001;3:203–213.
33. Mohan RM, Heaton DA, Danson EJ, Krishnan SP, Cai S, Channon KM *et al.* Neuronal nitric oxide synthase gene transfer promotes cardiac vagal gain of function. *Circ Res* 2002;91:1089–1091.
34. Li JM, Gall NP, Grieve DJ, Chen M, Shah AM. Activation of NADPH oxidase during progression of cardiac hypertrophy to failure. *Hypertension* 2002; 40:477–484.
35. Nediani C, Borchi E, Giordano C, Baruzzo S, Ponziani V, Sebastiani M *et al.* NADPH oxidase-dependent redox signaling in human heart failure: relationship between the left and right ventricle. *J Mol Cell Cardiol* 2007;42:826–834.
36. Shinyashiki M, Pan CJ, Lopez BE, Fukuto JM. Inhibition of the yeast metal reductase heme protein fre1 by nitric oxide (NO): a model for inhibition of NADPH oxidase by NO. *Free Radic Biol Med* 2004;37: 713–723.
37. Matsuura W, Sugimachi M, Kawada T, Sato T, Shishido T, Miyano H *et al.* Vagal stimulation decreases left ventricular contractility mainly through negative chronotropic effect. *Am J Physiol* 1997;273: H534–H539.
38. Mark AL. Sensitization of cardiac vagal afferent reflexes at the sensory receptor level: an overview. *Fed Proc* 1987;46:36–40.

Magnetic Resonance in Medicine 57:806–811 (2007)

Advantageous Application of a Surface Coil to EPR Irradiation in Overhauser-Enhanced MRI

Shingo Matsumoto,[1] Kenichi Yamada,[1] Hiroshi Hirata,[2] Keiji Yasukawa,[1] Fuminori Hyodo,[1] Kazuhiro Ichikawa,[1] and Hideo Utsumi[1]*

The present study describes the advantageous application of a surface coil to electron paramagnetic resonance (EPR) irradiation in Overhauser-enhanced MRI (OMRI). OMRI is a double-resonance method for imaging free radicals based on the Overhauser effect. Proton NMR images are recorded without and with EPR irradiation of the free radical resonance, which results in a difference proton image that shows signal enhancement in spatial regions that contain the free radical. To obtain good signal enhancement in OMRI, very high RF power and a long EPR irradiation time are required. To improve sensitivity and shorten the image acquisition time, especially for localized (and topical) applications, we developed and tested a surface-coil-type EPR irradiation coil. Theoretical calculations and experimental data showed that EPR irradiation through the surface coil could ameliorate the localized Overhauser enhancement, which was related to the ratio of B_1 surface coil/B_1 volume coil in the region of interest (ROI), as expected. The increased sensitivity could also be converted into a shortened EPR irradiation time, resulting in fast data acquisition. For biomedical applications, the use of a surface coil (as opposed to a conventional volume coil) could decrease the total RF power deposition in the sample required to obtain the same Overhauser enhancement in the ROI. Magn Reson Med 57:806–811, 2007. © 2007 Wiley-Liss, Inc.

Key words: dynamic nuclear polarization; free radical; imaging; OMRI; PEDRI; surface coil

There has been considerable interest in developing imaging techniques to determine the distribution of free radicals in biological tissues because of their implications for physiological and pathological conditions (1–4). Overhauser-enhanced MRI (OMRI), which is also called proton electron double-resonance imaging (PEDRI), is a novel technique for imaging free radicals in biological samples that is based on dynamic nuclear polarization (DNP) (5–8). A proton NMR image is recorded immediately following the irradiation of the electron paramagnetic resonance (EPR) of free radicals associated with the system, resulting in a signal-enhanced proton image. Recent studies have successfully expanded this technique to obtain functional information, including noninvasive pO_2 maps and simultaneous images of different redox reactions (6,9). OMRI can provide high spatial resolution independently of the linewidth of the paramagnetic species, but the enhancement of the NMR signal will depend on the local concentration of the free radical. Therefore, OMRI is capable of indirectly imaging free-radical distribution in large conducting samples, potentially even in humans. The large conducting samples, however, absorb a significant amount of radiofrequency (RF) power needed for the EPR irradiation. The unpaired electron in the sample absorbs only a small percentage of the RF power applied, resulting in a significant loss of sensitivity and hence a long EPR irradiation time.

Surface coils are widely used in MR studies because of their superior performance in limited target regions (10–13). In most conventional MRI techniques, surface coils are used as the receiver coil because the sensitivity of MRI depends mainly on the conversion factor of the receiver, not the irradiation coil. The use of a surface-coil-type receiver coil for NMR detection may be also beneficial in OMRI to improve the signal-to-noise ratio (SNR). The application of a surface coil to NMR detection does not affect the contrast enhancement ratio (the ratio of the NMR signal with EPR irradiation/without EPR irradiation). For imaging paramagnetic material with a large linewidth or a lower concentration, especially in biomedical applications, modification of the contrast enhancement ratio may be more crucial than the improvement of NMR detection efficiency. In the present study we constructed and tested a surface-coil-type EPR irradiation coil for OMRI. The design and characteristics of the OMRI surface coil were based on that for low-frequency EPR system previously described (14–16). Such an approach would be useful for improving the contrast enhancement ratio in OMRI, especially for a limited target region in a large conducting sample.

MATERIALS AND METHODS

OMRI Scanner and Pulse Sequence

The OMRI experiments were performed on a custom-built OMRI scanner (POEM; Philips Research Laboratories, Hamburg, Germany; Fig. 1a) with a horizontally oriented human whole-body magnet (79-cm diameter, 125-cm length). The ramp time of the main magnet required to change the B_0 field from 8 mT to 15 mT with homogeneity of ±5 μT on a 400-mm DSV (diameter spherical volume) was <5 ms. The NMR resonator assembly consisted of a transmit saddle coil (25-cm diameter, 23-cm length) and a solenoidal receive coil (7-cm diameter, 6-cm length) tuned to 617 kHz. A saddle coil (13.5-cm diameter, 23.5-cm length) tuned to a frequency of 221 MHz was used as a

[1]Department of Biofunctional Science, Graduate School of Pharmaceutical Sciences, Kyushu University, Fukuoka, Japan.

[2]Department of Electrical Engineering, Yamagata University, Yonezawa, Yamagata, Japan.

Grant sponsors: Japan Society for the Promotion of Science; Ministry of Education, Culture, Sports, Science and Technology of Japan.

*Correspondence to: Prof. Hideo Utsumi, Department of Biofunctional Science, Graduate School of Pharmaceutical Sciences, Kyushu University, Fukuoka 812-8582, Japan. E-mail: utsumi@pch.phar.kyushu-u.ac.jp

Received 8 May 2006; revised 5 December 2006; accepted 22 December 2006.

DOI 10.1002/mrm.21198

Published online in Wiley InterScience (www.interscience.wiley.com).

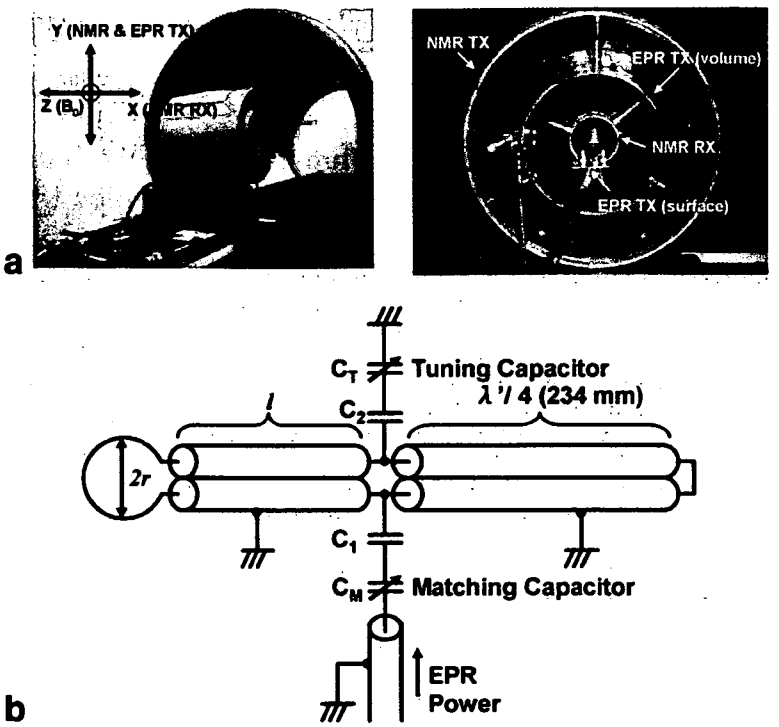

FIG. 1. **a:** Pictures and geometric orientation of the main magnet and RF coil assembly. **b:** Configuration of a surface-coil-type EPR irradiation coil for OMRI with matching and tuning circuits. The length of the parallel coaxial line was 158 mm, the radius of the surface coil was 10 mm, and the thickness of the wire used for the surface coil was 2.0 mm. The value of the capacitors C_1 and C_2 was 3.0 pF. The capacitance of the trimmer capacitors C_M and C_T was variable from 0.8 to 10 pF. The semi-rigid coaxial cables were used for the parallel line and the balun.

volume coil for EPR irradiation. It was placed concentric to and in between the NMR transmit and receive coils. The conversion efficiency of the RF magnetic field for the EPR irradiation was 5.4 $\mu T/W^{1/2}$, and the characteristics of the volume coil in terms of EPR irradiation efficiency and RF power deposition were compared with those of the surface coil, as described below.

We performed the OMRI experiments using a standard MRI gradient-echo sequence in which each phase-encoding step was preceded by an EPR saturation pulse to elicit the Overhauser enhancement. The pulse sequence started with the B_0 field at 7.5 mT, corresponding to the EPR frequency. The EPR irradiation was then switched on for a period of about 400 ms. The B_0 field was ramped up to 14.5 mT before the application of the NMR pulse and associated field gradients, and the echo signals were acquired. The scan parameters were as follows: matrix size = 64 × 64, field of view (FOV) = 64 × 64 mm^2, repetition time (TR) = 1200 ms, echo time (TE) = 25 ms, and EPR pulse length (TEPR) = 400 ms. The images were reconstructed from the echoes by means of the standard software implemented in the system.

Basic Design of the Surface Coil for EPR Irradiation

The configuration of the surface-coil-type EPR irradiation coil was similar to that previously described for continuous-wave EPR spectroscopy (14–16). The resonant circuit consisted of a single-turn loop coil, a parallel coaxial line formed by 50-ohm coaxial cables (MCT-358T; Miyazaki Electric Wire & Cable Co., Kanagawa, Japan), a half-wave line balun, and trimmer capacitors (variable range = 0.8–10 pF, rated voltage = 250 VDC; Johanson Manufacturing Co., Boonton, NJ, USA) for matching and tuning as shown in Fig. 1b. The operating frequency of the surface coil was designed to have an EPR irradiation frequency of 221 MHz for OMRI.

The specifications of the surface coil are shown in Table 1. The trimmer capacitors can tune the resonant frequency in the range of ±4 MHz with 50-ohm impedance matching. All measurements were performed with appropriate impedance matching, in which the reflection coefficient S_{11} was less than –30 dB. The generation efficiencies Λ of the RF magnetic field of both volume and surface coils were determined using a small-loop antenna (17,18).

Table 1
Specifications of EPR Irradiation Coils

Specifications	Volume coil	Surface coil
Structure	Saddle	Single-turn-loop
Operating frequency	221 MHz	221 MHz
Diameter of coil	135 mm	20 mm
Length of coil	235 mm	2 mm
Length of transmission line	—	158 mm
Length of balun (total)	—	234 mm (468 mm)
$Q_{unloaded}$	210	218
$Q_{test\ tube\text{-}loaded}$	198	176
$Q_{rat\ loaded}$	140	Noninvasive 126[a]; invasive 66[b]
Generation efficiency of RF magnetic field[c]	5.4 $\mu T/W^{1/2}$	23.9 $\mu T/W^{1/2}$

[a]Surface coil was placed on the flank without surgery.
[b]Surface coil was directly fixed on the left kidney of rat after abdominal operation.
[c]Measured for the unloaded RF coils.

Overhauser Effect and RF Power Deposition

In the Overhauser effect (also known as DNP), the electron spin polarization is transferred to the proton while an EPR of the paramagnetic species is irradiated, resulting in the enhancement of NMR signal. The enhancement factor E is defined as the ratio of measured NMR signal intensity with and without EPR irradiation, which is given by

$$E = 1 - (\gamma_e/\gamma_p) f k \frac{s}{n} \quad [1]$$

where γ_e and γ_p are respectively the electron and proton gyromagnetic ratios, and the absolute value of their ratio is equal to 658 (6). The leakage factor f accounts for the fraction of nuclear relaxation caused by the presence of the paramagnetic contrast agent. The coupling factor k depends on the nature of the interaction between the contrast agent and the protons, and n is the number of EPR lines split by the hyperfine coupling. The saturation factor s is the amount of saturation of the EPR resonance, which can be written as

$$s = \frac{\gamma_e^2 B_{1e}^2 T_{1e} T_{2e}}{1 + \gamma_e^2 B_{1e}^2 T_{1e} T_{2e}} \quad [2]$$

where B_{1e} is the RF magnetic field for EPR (6), and T_{1e} and T_{2e} are the longitudinal and transverse electron spin relaxation times, respectively, which mainly depend on the concentrations of the contrast agent and the oxygen. Taking all the factors in Eq. [1] and [2] into account, the Overhauser effect is only dependent on the RF magnetic field for EPR if the OMRI is performed with the same sample, dosage of contrast agent, and pulse sequence. B_{1e} is defined by the RF magnetic field generation efficiency of the coil (i.e., the structure of EPR irradiation coil) and by the square root of the RF power supplied to the coil. One can experimentally determine the amount of RF power deposited in the conducting sample P_{sample} by measuring the amount of RF power dissipated in the sample (19). Using loaded and unloaded coil quality factors (Q_{loaded} and $Q_{unloaded}$, respectively), one can calculate the power deposited in the conducting sample as

$$P_{sample} = P_{total}\left(1 - \frac{Q_{loaded}}{Q_{unloaded}}\right) \quad [3]$$

where P_{total} is the total RF power supplied to the RF coil. Accordingly, one can predict the advantage of the surface coil (compared to a volume coil) for reducing the total RF power absorbed by the body during EPR irradiation by calculating and comparing the amount of RF power deposited in the sample required to obtain the same Overhauser enhancement.

OMRI Measurements

A test tube (inner diameter = 14 mm, height = 26 mm) containing 3 mM of carbamoyl-PROXYL (Sigma Co., St. Louis, MO, USA) dissolved in physiological saline solution was imaged. Gradient-echo OMRI data sets were obtained at various EPR irradiation powers with a surface coil or a volume coil. The EPR RF power output from the amplifier (model 5001L; Electronic Navigation Industries, USA) used for the calculation was based on the actual output power measured experimentally. It was linear until 100 W and then became lower than the setting value in the range of >100 W. We obtained a difference image by subtracting the data sets without EPR from those with EPR, which revealed the distribution of the free radical under study. The enhancement factor E was calculated from the value at the center of the surface coil (i.e., the loop plane) and at various distances from the loop plane on the x-z images as the ratio of NMR signal intensity with and without EPR irradiation.

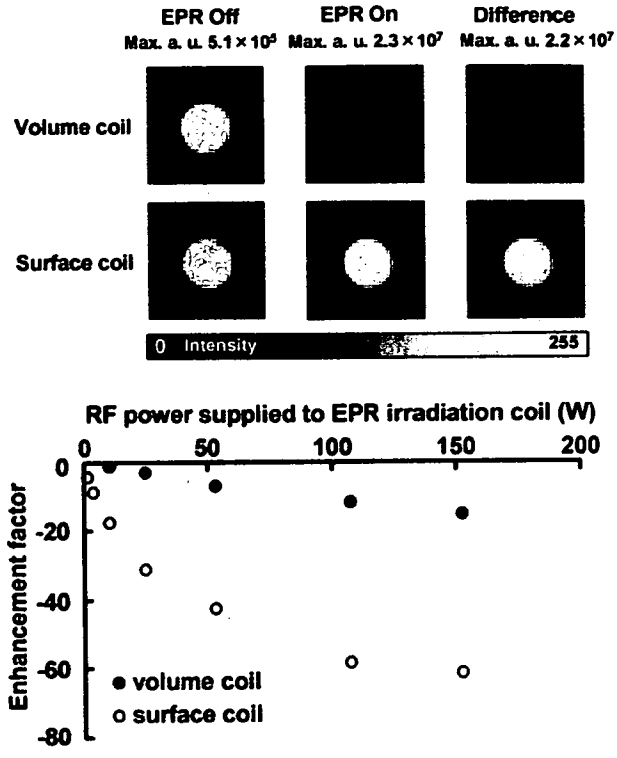

FIG. 2. Comparison of the enhancement factor between the surface and volume coils at different RF power levels using an RF power amplifier (model 5001L; Electronic Navigation Industries, USA). x-z Slice OMRI images of 3-mM carbamoyl-PROXYL solution were obtained with and without EPR irradiation using a volume coil or a surface coil for EPR irradiation. A difference image was obtained by subtracting images obtained with and without EPR irradiation. The enhancement factor E was calculated as the ratio of NMR signal intensity measured from images with and without EPR irradiation. The negative sign of E indicates that the NMR signal changes phase by 180° upon irradiation of the EPR resonance.

Male Wistar rats were obtained from Seac Yoshitomi Co. (Fukuoka, Japan). The rats were 6 weeks old and weighed 180–200 g at the time of the experiments. They were laid on their side and anesthetized by intraperitoneal injection of pentobarbital. The rat-loaded quality factor was measured with the use of a network analyzer (R3765BG; Advantest Co., Tokyo, Japan) before the imaging experiments were conducted. Then 0.8 mmol of carbamoyl-PROXYL